Tetramerization of the DNA mismatch repair protein MutS enhances daughter strand incision preferentially in the vicinity of replication errors

Mardenborough, Yannicka; van Genderen, Romano M.; Laffeber, Charlie; de Koning, Kelly D.A.; Friedhoff, Peter; Kanaar, Roland; Depken, Martin; Lebbink, Joyce H.G.

DOI
10.1016/j.jbc.2025.110881

Licence
CC BY-NC-ND

Publication date
2025

Document Version
Final published version

Published in
Journal of Biological Chemistry

JBC RESEARCH ARTICLE

Tetramerization of the DNA mismatch repair protein MutS enhances daughter strand incision preferentially in the vicinity of replication errors

Received for publication, June 26, 2025, and in revised form, October 12, 2025 Published, Papers in Press, November 4, 2025
https://doi.org/10.1016/j.jbc.2025.110881

Yannicka Mardenborough[1], Romano M. van Genderen[1], Charlie Laffeber[1], Kelly D. A. de Koning[1], Peter Friedhoff[2], Roland Kanaar[1], Martin Depken[3], and Joyce H. G. Lebbink[1,4,*]

From the [1]*Department of Molecular Genetics, Oncode Institute, Erasmus MC Cancer Institute, Erasmus University Medical Center, Rotterdam, The Netherlands;* [2]*Institute for Biochemistry, FB 08, Justus-Liebig University, Giessen, Germany;* [3]*Kavli Institute of NanoScience and Department of BionanoScience, Delft University of Technology, Delft, The Netherlands;* [4]*Department of Radiotherapy, Erasmus MC Cancer Institute, Erasmus University Medical Center, Rotterdam, The Netherlands*

Reviewed by members of the JBC Editorial Board. Edited by Patrick J. O'Brien

DNA replication errors that escape the proofreading activity of the replicative DNA polymerase are repaired by DNA mismatch repair (MMR). The initiation of MMR in *Escherichia coli* involves the recognition of the mismatch by MutS, binding of MutL, and activation of the endonuclease MutH which incises DNA at a hemi-methylated GATC site. MutS exists in a dimer-tetramer equilibrium, but the function of the tetramer during MMR remains unknown. Here, we used *in vitro* MutH activation assays to examine the role of MutS in the reaction steps that couple mismatch recognition to daughter strand incision. To study the behavior of different MutS oligomers, we used obligate dimers and tetramers and quantified GATC site incision on circular and linear DNA substrates. Especially in the presence of free DNA ends, MutS tetramers mediate more efficient incision than MutS dimers, likely due to tetramers diffusing slower and therefore being more successful in assembling the active incision complex before dissociating from the DNA at the ends. Likewise, we observed that MutS tetramers have a higher preference for nicking the GATC site close to the mismatch than dimeric MutS. Through probabilistic modeling, we show that this increased preference is consistent with a fourfold decrease in diffusion constant for the tetramer compared to the dimer. We propose that during mismatch repair, DNA excision tracts resulting from MutS tetramer-mediated incision will be shorter than those mediated by the dimer, and that this explains the reported higher repair efficiencies of wild-type MutS compared to the dimer.

DNA mismatch repair (MMR) maintains genome stability through the repair of base-base mismatches and small insertion-deletions loops that arise during DNA replication (1, 2). MMR is an evolutionarily conserved process (1), and loss of function in MMR proteins leads to a mutator phenotype and is associated with predisposition to cancer (Lynch syndrome) in humans (3). The MMR pathway of *Escherichia coli* was the first to be reconstituted *in vitro* (4) and the process has since been well defined. During the initiation of MMR in *E. coli*, MutS recognizes the mismatch (5, 6), undergoes an ATP-dependent conformational change (7–10) and then recruits MutL to DNA (7, 11–13). In an ATP-dependent manner, MutL subsequently activates the endonuclease activity in MutH, which then incises the DNA daughter strand (14, 15). *E. coli* and other γ-proteobacteria use transiently hemi-methylated GATC sites to differentiate between the parental and daughter strand (16). GATC sites are methylated by *dam* methylase, and the methylation activity lags behind DNA replication by approximately 1 min (17, 18). This delay provides a short window in time during which MutH must incise the newly synthesized, unmethylated strand at the hemi-methylated GATC site (19). The incision allows subsequent removal of the strand containing the incorrect nucleotide by helicase and exonucleases, after which resynthesis takes places (1, 2).

Mismatch binding by homodimeric MutS or heterodimeric MutS homologs results in an ATP-binding-dependent conformational change to a ring-like structure that can rapidly diffuse along DNA as a sliding clamp (8, 13, 20–22). In *E. coli*, each subunit of MutS contains 853 amino acids in which the last 53 amino acids of the C-terminus are involved in dimer stabilization and tetramer formation (23, 24). However, this tetramer formation is reversible which causes MutS to exist in a dynamic dimer–tetramer equilibrium, with reported dissociation constants in the range of 50 nM–2 μM (23, 25). Tetramerization is further stimulated by DNA binding (23, 26, 27).Tetramers have not been observed for the eukaryotic MutS homologs MutSα and MutSß, although MutSß and *E. coli* MutS share a similar double helix-loop-helix fold in their C-termini (28). A recent study using atomic force microscopy reported that MutSα-mismatched DNA complexes, in the presence of ATP, often contain two MutSα dimers (29). The authors suggest that the conformational change to the sliding clamp might enable MutSα-MutSα interactions.

The precise role of MutS tetramers in MMR has not been determined. A variant of the gene for MutS with a C-terminal

* For correspondence: Joyce H. G. Lebbink, j.lebbink@erasmusmc.nl.

truncation that is unable to form tetramers (MutSΔC800) complements a *mutS* null *E. coli* strain when overexpressed (30). When this gene is integrated into the *E. coli* genome and thus is expressed from a single copy, there are severe MMR defects, indicating that the C-terminal 53 amino acids are important (31). The gene for MutS D835R, a constitutive dimer, results in similar rates of mutations as MutSΔC800 when overexpressed in a *mutS* null strain (24). However, another study showed that incorporating the MutS D835R mutant into the *E. coli* genome had a weak mutator phenotype compared to the strong defects of MutSΔC800 (32). This suggests that the defects observed with MutSΔC800 cannot solely be attributed to a lack of tetramer formation. Therefore, while MutS tetramerization plays a role in MMR, it is not essential.

MutS tetramers are involved in MMR-mediated inhibition of homologous recombination (anti-recombination) (30). Mismatches formed during the recombination of non-identical DNA sequences are bound by MutS. MutS and MutL physically restrict strand exchange by also binding the secondary structures in single-stranded (ss)DNA that has been displaced during the formation of recombination intermediates (33). Anti-recombination defects in *mutS* null *E. coli* are more pronounced when MutSΔC800 is overexpressed compared to wild-type MutS (30). In *in vitro* recombination assays, MutSΔC800 was also less efficient at inhibiting homologous recombination than wild type (33). MutS tetramers have two DNA binding sites (26, 27, 34) which would allow the protein to bind both the heteroduplex region of recombination intermediates and the displaced ssDNA simultaneously. Taken together, this indicates that MutS tetramers are important for anti-recombination.

The exact mechanism that couples mismatch recognition by MutS to strand incision by MutH is unresolved. Several models have been proposed including the polymerization model wherein MutL accumulates from the mismatch to the strand discrimination signal (29, 35–38), static transactivation wherein protein mediated loops connect the mismatch to the GATC site (39, 40), active translocation driven by ATP (hydrolysis) by MutS (41, 42) and the molecular switch model wherein proteins diffuse along DNA in an ATP hydrolysis-independent manner (13, 20, 43, 44). There is increasing support for a (diffusive) mode of communication along the DNA backbone (22, 44–48). Because MutS tetramers display higher avidity for DNA and dissociate slower than dimeric MutS (34), it is possible that the MutS oligomerization state will influence (diffusive) communication along the DNA helix. So far this has not yet been explicitly studied.

This study aims to investigate the mode and relevance of communication along the DNA helix and the possible role of MutS tetramer formation during this process. We functionally analyzed MMR initiation, *i.e.*, DNA daughter strand incision, using *in vitro* MutH activation assays. By using MutS D835R, an obligate dimer that is unable to form tetramers, as well as crosslinked MutS tetramers, we were able to examine the behavior of MutS dimers and tetramers separately. We show that MutS tetramers enable more efficient incision than MutS dimers, especially in the presence of free DNA ends. Furthermore, we show that MutS tetramers encourage preferential incision of GATC sites near the mismatch and that a model based on Fickian diffusion can correctly predict these preferences while returning different diffusion constants for MutS dimers and tetramers. We discuss the possible implications of these findings for DNA MMR.

Results

GATC site incision on circular and linear DNA

We have previously provided evidence for communication between the mismatch and the hemi-methylated GATC sites during MMR in *E. coli* occurring along the DNA backbone (48). Similar to earlier published work by Modrich and colleagues (47), we showed that DNA roadblocks placed in between a mismatch and hemi-methylated GATC sites severely reduce incision activity. Furthermore, we established that residual activity could be fully attributed to the long, disordered linkers in MutL that allow roadblock bypass. In addition to studying the effect of placing a roadblock in between the mismatch and GATC site, Modrich and colleagues also showed that a double strand break in the short path between the mismatch and the unique GATC site on their 6 kb substrate (but not in the long path) significantly impairs strand incision by MutH, likewise indicating that communication occurs along the helix (14, 47). Here we further examined the effect of free DNA ends on MutH activation by investigating strand incision on circular and linear DNA substrates. We used our previously established MutH activation assay in which we followed simultaneous strand incision of two hemi-methylated GATC sites flanking a G/T mismatch on a 3 kb linear and circular DNA substrate labelled with an Alexa^{647} fluorophore (48, 49). On this GT#2 substrate, GATC site one is located 1042 bp 3′ of the mismatch and GATC site two is located 31 bp 5′ of the mismatch (Fig. 1). DNA substrates (0.5 nM) were mixed with 10 nM wild-type MutS, 10 nM MutL, and 5 nM MutH (concentrations refer to monomers) in the presence of ATP and reaction products were analyzed *via* denaturing agarose electrophoresis as described previously (48). In the absence of DNA ends we observed complete incision of the circular DNA substrate within 5 min (Fig. 1). Approximately 10% of the substrate was incised once (either GATC site one or GATC site 2), but the majority of the incised products contained two nicks. This corresponds to our previous results which showed that intermediate products containing a single nick are immediately converted to double-nicked products (49). On linear DNA, only a negligent amount of fully nicked product is produced within 5 min (Fig. 1). Likewise, the amount of intermediate products is very low. However, we did note a very slight preference for GATC site 2, similar to what we previously observed at higher protein concentrations (50 nM MutS, 50 nM MutL and 25 nM MutH) on linear DNA (48). The sensitivity of incision activity to DNA ends suggests that MutS, MutL and/or the MutSL complex move along the DNA helix and dissociate off the DNA ends before incision can occur. Our data on a 3 kb DNA

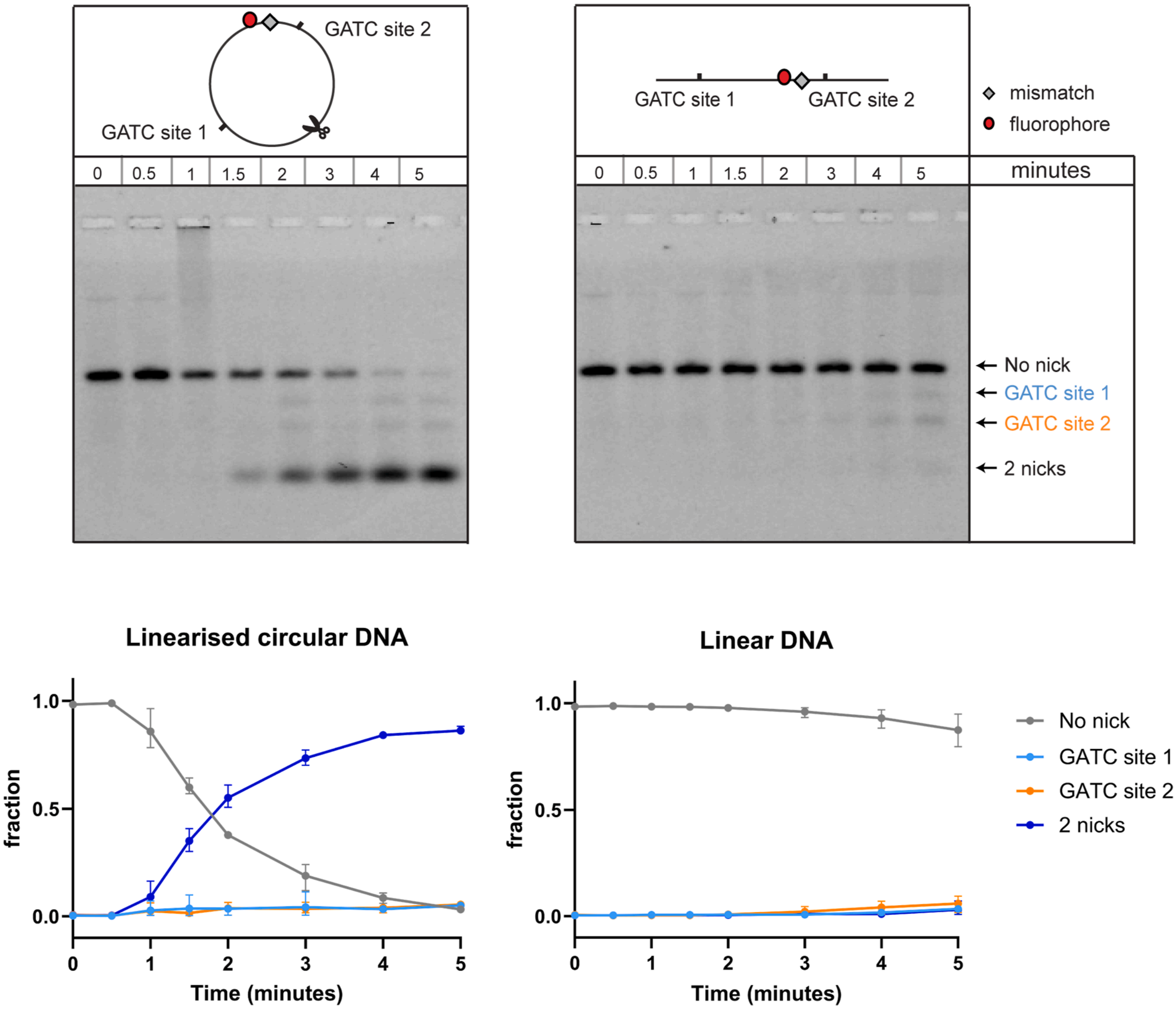

Figure 1. Efficiency of daughter strand incision is sensitive to the presence of DNA ends. Time courses for strand incision by 10 nM wild-type MutS, 10 nM MutL and 5 nM MutH on 0.5 nM 3 kb circular (*left*) and linear (*right*) GT#2. Following incision, the circular DNA substrates were linearized by ScaI. Reaction products were separated using gel electrophoresis under denaturing conditions and visualized using Alexa^{647} fluorophore emission. Graphs underneath the gels show fractions of reaction products containing no nick (*gray*), a nick at GATC site 1 (*light blue*), a nick at GATC site 2 (*orange*) and both sites nicked (*dark blue*). Data points with error bars indicate mean value and range over three independent experiments.

substrate with two GATC sites flanking the mismatch thus corresponds to the findings of the Modrich laboratory that a double-strand break between the mismatch and a single GATC site on a 6 kb DNA substrate impairs strand incision (14, 47).

The MutS concentration influences incision on linear substrates more than MutL and MutH concentrations

On our linear substrate, the mismatch is flanked by GATC sites. Thus, the reduced incision activity can only be due to proteins dissociating from the ends of the DNA if they have failed to form the activated incision complex before passing over GATC site. This would be possible if the rates for protein complex formation and/or conformational changes required for activation of the endonuclease, are slow on the timescale of movement of individual proteins or protein complexes along the DNA backbone. Because all protein concentrations are in molar excess over the 3 kb DNA substrate, multiple MutS and MutL molecules can be loaded during the experiment. Both MutS and MutL have been observed to diffuse along DNA (22, 44–46). MutS-MutL complexes diffuse slower than MutS clamps on their own (44), and MutL has been shown to prevent MutS clamps from leaving the mismatch (10, 40). Therefore, increased concentrations of MutL should provide more opportunities for MutS-MutL complex formation and keep MutS on DNA. Additionally, MutL releases from MutS while on DNA (22, 44) and activates MutH on its own (48). Therefore, it is possible that increasing the amount of MutL in the reaction mixture will also increase the number of MutL clamps simultaneously present on the same DNA molecule.

We first attempted to reduce the number of individual proteins falling off the DNA ends through increasing the rate of protein complex formation by raising protein concentrations. Indeed, when we increased the concentration of MutL or MutH, we observed more efficient incision on linear DNA (Fig. 2, *A* and *B*). However, in contrast to incision on circles, the reaction on linear DNA did not reach completion within 5 min. Compared to the amount of substrate incised by 10 nM MutS, 10 nM MutL, and 5 nM MutH, incision at 200 nM MutL or 100 nM MutH only increased twofold.

In contrast, upon increasing MutS concentration, we observed a near-immediate increase in incision efficiency (Fig. 2*C*). Complete incision of linear DNA within 5 min was already observed at a concentration of 50 nM MutS, with saturating behavior at 100 nM MutS. These results indicate that incision activity in the presence of DNA ends is more dependent on MutS than MutL or MutH.

MutS tetramers are more efficient in activating MutH than MutS dimers

Because increasing the concentration of MutS in the reaction mixture from 10 to 200 nM will shift its oligomerization equilibrium from dimer toward tetramer (23, 25), we investigated whether MutS oligomerization influences incision efficiency. To investigate the specific roles of MutS dimers and tetramers, we used obligate oligomeric variants of the wild-type protein to uncouple incision from the oligomerization equilibrium. We used the mutant MutS D835R which forms obligate dimers (24, 32, 34), and we created obligate MutS tetramers from single cystein MutS dimers that have been crosslinked at the position C848 (34). Crosslinking of the MutS tetramers occurred efficiently (Fig. S1*A*). We compared MutS D835R, crosslinked MutS tetramers, and wild-type MutS by using the same monomer concentration for each variant, which means that at 10 nM MutS, we are comparing 5 nM dimer with 2.5 nM tetramer. However, this is the most controlled way to compare each condition as we cannot determine the actual oligomeric status of the wild-type MutS during the experiment.

We first verified that all MutS variants are functional by observing incision on circular mismatched DNA at low protein concentrations (10 nM MutS, 10 nM MutL, 5 nM MutH) (Fig. 3*A* left panel). We also measured the background activity for each MutS variant by observing incision on substrates without a mismatch. At low protein concentrations (10 nM MutS, 10 nM MutL, 5 nM MutH), wild-type MutS and MutS D835R converted less than 10% of the homoduplex complex (Fig. S1*B*). However, at the same protein concentration, MutS tetramers showed about 30% incision. At higher protein concentrations (100 nM MutS, 100 nM MutL, and 50 nM MutH), background incision was only slightly higher than at low protein concentrations (Fig. S1*C*). Taken together, all MutS oligomeric variants are able to activate MutH in a predominantly mismatch-specific manner.

On circular DNA substrates with a GT mismatch, all variants were able to achieve full conversion (of at least 1 GATC site) within the 10-min timeframe of the reaction at 10 nM MutS, 10 nM MutL, and 5 nM MutH (Fig. 3*A* left panel). We observed about twofold slower incision for MutS D835R than wild-type MutS and two-fold faster incision for the obligate tetramer. The observed differences are relatively small but reproducible and correspond to previous studies reporting the non-essential role of MutS tetramers for *in vivo* mismatch repair efficiency (24, 32).

Interestingly, if we perform the experiment on linear DNA rather than on circles, at otherwise identical reaction conditions, we observe a much larger effect of the MutS oligomeric state (Fig. 3*A* right panel). As expected (Fig. 1), reduced incision activity was observed with wild-type MutS, with only approximately 40% of the linear substrate being incised within 10 min. With the obligate tetramer, incision is still complete within the timeframe of the reaction, with half of the substrate already converted within the first 90 s. In contrast, the obligate dimer MutS D835R showed no observable activity at all. These relative differences of incision activity on linear DNA are much larger than those on circles. Similar to wild-type MutS, increasing the concentrations of MutL and MutH only marginally increased incision activity for the dimer (Fig. 3*B* right panel). Also, while increasing the wild-type MutS concentration resulted in a large increase in efficiency (Fig. 3*B* left panel), titrating dimeric MutS never results

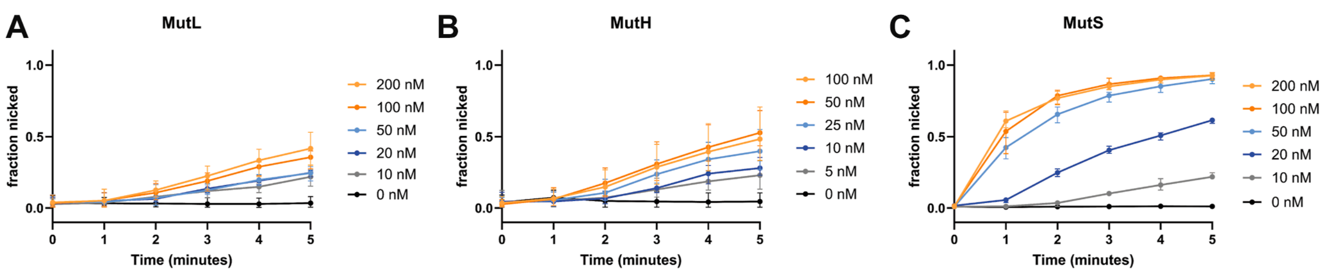

Figure 2. MutS concentration has a larger effect on incision of linear DNA than MutL or MutH concentrations. Graphs show time courses of the fraction of nicked DNA (all nicked species so either one or both sites nicked) for various protein concentrations. *A*, MutS wild-type and MutH concentrations remain at 10 nM and 5 nM respectively and MutL is titrated as indicated in the legend. *B*, MutS wild-type and MutL concentrations remain at 10 nM and MutH is titrated. *C*, MutL and MutH concentrations remain at 10 nM and 5 nM respectively and MutS wild-type is titrated as indicated. Data points with error bars indicate mean value and range over three independent experiments.

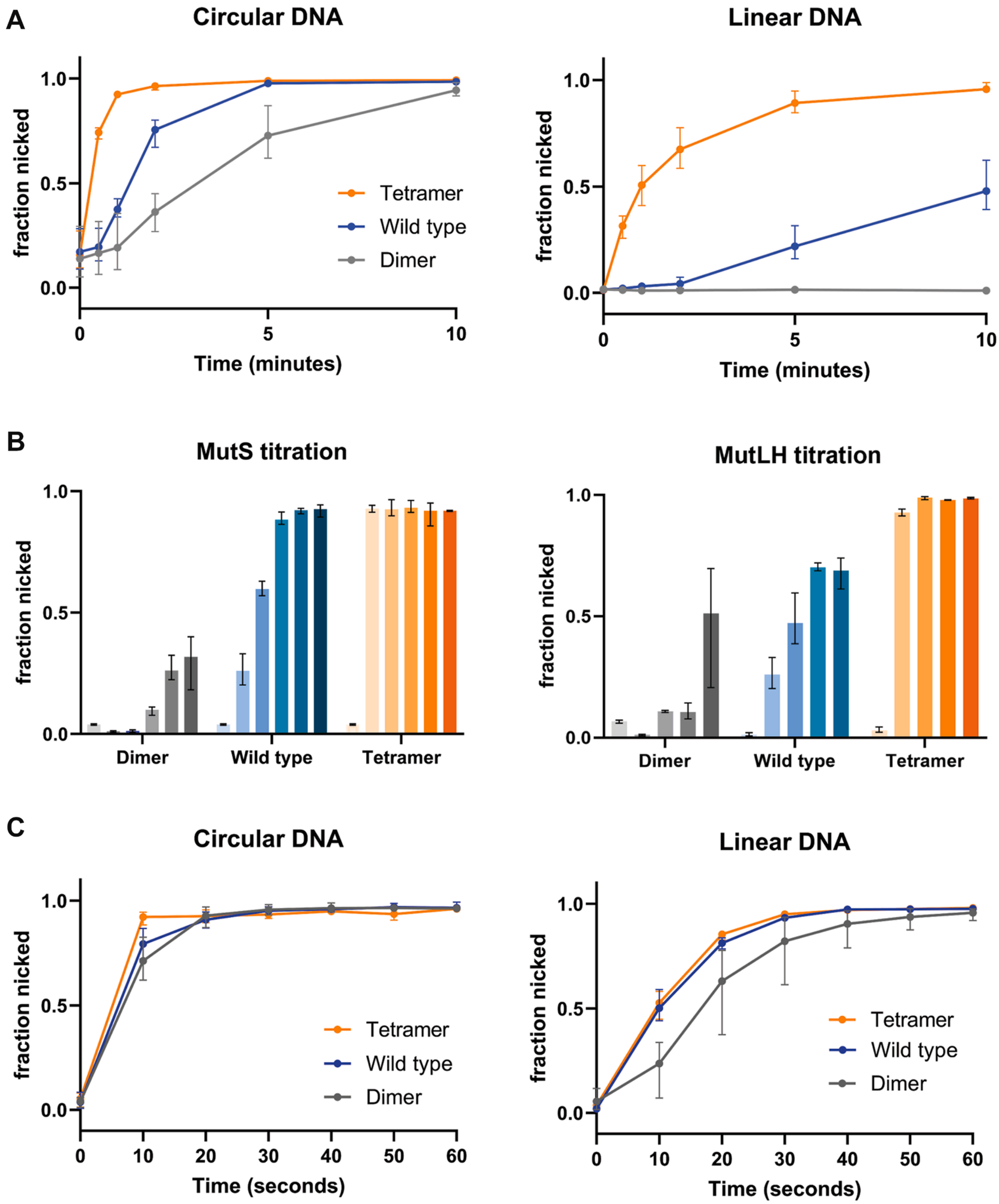

Figure 3. MutS dimers and tetramers behave differently on DNA. *A*, time courses for strand incision by 10 nM MutS, 10 nM MutL and 5 nM MutH on 0.5 nM 3 kb circular (*left panel*) or linear (*right panel*) GT#2 for MutS dimer (*grey*), wild type (*blue*) and tetramer (*orange*). *B*, *Left panel*; Fraction of incised linear substrate at 5 min for MutS dimer, wild type and crosslinked tetramer as function of increasing concentration of MutS (from *light* to *dark* color 0 nM, 10 nM, 20 nM, 50 nM, 100 nM and 200 nM), while MutL and MutH are kept at 10 nM and 5 nM respectively (n = 3). Wild type values were taken from the experiment featured in Figure 2. *Right panel*; Fraction of incised linear substrate at 5 min for MutS dimer, wild type and crosslinked tetramer with 10 nM MutS as function of increasing concentrations of MutL (from *light* to *dark* color 0 nM, 10 nM, 100 nM, 200 nM, 500 nM) and MutH (half of MutL concentration) (n = 3). *C*, time courses for strand incision by 500 nM MutS, 500 nM MutL and 250 nM MutH on 0.5 nM circular (*left panel*) or linear (*right panel*) GT#2 (n = 3). Dimer is shown in *grey*, wild type in *blue*, and tetramer in *orange*. Fraction nicked refers to all nicked species so either one or both GATC sites modified. Data points with error bars indicate mean value and range.

in complete conversion (Fig. 3*B* left panel). Simultaneously increasing MutS, MutL, and MutH concentrations causes the obligate dimer to become active and obscures the difference between both DNA topology and MutS oligomeric variants (Fig. S1*D*). These findings indicate that (1) the dynamic oligomerization equilibrium shifts from dimer to tetramer when wild-type MutS concentration increases; (2) efficiency of incision on linear DNA is much more dependent on the oligomeric state of MutS than incision efficiency on DNA circles, suggesting that MutS tetramers diffuse relatively slowly and remain on DNA long enough to enable the formation of an activated incision complex while MutS dimers diffuse off the free end of the DNA prematurely; and (3) multiple loading of MutS and MutL enhances the residence time of MutS dimers on DNA long enough to allow MutH activation.

MutS tetramers preferentially incise the GATC site close to the mismatch

On linear GT#2 DNA, we previously noted that wild-type MutS displays a slight preference for activating incision of the GATC site that is closest to the mismatch: GATC site two at 31 bp from the mismatch as compared to GATC site one at 1042 bp from the mismatch (Fig. 1). We also observed this site preference more clearly in our previously reported experiments using concentrations of 50 nM wild-type MutS, 50 nM MutL, 25 nM MutH (48). Since the abovementioned results suggest that MutS tetramers diffuse slower along DNA than MutS dimers, we studied whether tetramer formation affects the preferential incision of GATC sites on DNA substrates with the G/T mismatch and the GATC sites in two different configurations (Fig. 4). To be able to best determine the effect of MutS oligomerization, we performed incision assays at 10 nM MutS, 500 nM MutL, and 250 nM MutH so that MutL and MutH are at saturating conditions. Indeed, using substrate GT#2 under these conditions, we observed a strong preference for the GATC site close to the mismatch (GATC site 2; Fig. 4*A*). The effect is even more prominent with the MutS tetramer than with the MutS dimer (Fig. 4*C*).

We then changed the configuration of the DNA by moving the mismatch away from GATC site 2 and locating it closer to GATC site 1 (GT#2b; Fig. 4*B*). Surprisingly, site preference was no longer observed on GT#2b for the dimer. However, we did observe a clear switch in incision pattern with the tetramer (Fig. 4*B*), which now preferentially activates incision of GATC site one close to the mismatch (Fig. 4*C*).

To quantitatively confirm the site preference data, we created a probabilistic model in which the complex of MutS (dimers or tetramers), MutL and MutH is diffusing on GT#2 and GT#2b. The model determines the probabilities of finding inactive and active incision complexes on the DNA as a function of position and time, and allows us to calculate the incision probabilities of the individual GATC sites over time. By fitting the dimeric and tetrameric MutS diffusion constants, our Fickian diffusion model captures the experimental site preferences on both DNA substrates well (Fig. 4*D*). For the dimer, a diffusion constant D_2 of $(5.2 \pm 0.02) \times 10^{-3}$ $\mu m^2/s$ was obtained. For the tetramer, a 4.5 times smaller diffusion constant D_4 of $(1.4 \pm 0.06) \times 10^{-3}$ $\mu m^2/s$ was obtained. Taken together, these results indicate that the tetramer diffuses slower than the dimer, resulting in increased preference for incision of the GATC site closest to the mismatch.

Discussion

Communication along the DNA helix contour

There has been growing support for MMR models that describe communication between mismatch and GATC site along the DNA backbone, including single molecule experiments that monitor the movement of bacterial and yeast proteins (22, 44, 45). Functional studies that analyze *E.coli* endonuclease activation on hemimethylated GATC sites, including those performed in our laboratory, also provide evidence towards this hypothesis (47, 48). In the current study, we show that on linear DNA, incision is reduced compared to circular DNA substrates (Fig. 1). Because the only difference between the experimental conditions is the presence of free DNA ends, from which proteins may dissociate, this observation supports the hypothesis that communication occurs along the DNA backbone. However, the exact mechanism by which this communication occurs has not been established. The proposed models for communication along the DNA backbone include MutL polymerization (29, 35–38), active translocation of proteins driven by ATP hydrolysis (41, 42), and the molecular switch model wherein proteins diffuse along DNA in an ATP hydrolysis-independent manner (13, 20, 43, 44).

Support for ATP hydrolysis-independent diffusive movement along the DNA by MutS and MutL comes from a number of single molecule studies (22, 44, 50). In addition, both wild-type MutS as well as hydrolysis-deficient MutS have been shown to slide off free DNA ends in the presence of ATP (13, 20, 40, 51, 52). Therefore, the reduced incision efficiency observed in the presence of DNA ends may be due to MutS sliding clamps diffusing off the DNA ends before incision by MutH can occur. By increasing MutS concentration, we were able to increase incision efficiency on linear DNA more than by increasing MutL and MutH concentration (Fig. 2). MutS exists in a dynamic dimer-tetramer equilibrium and is more likely to form tetramers at higher protein concentrations and in the presence of DNA (23, 53, 54). Therefore, the strong dependence on MutS concentration implies a role of MutS tetramers in incision efficiency and diffusion along the DNA helix.

MutS tetramers modulate strand incision

The results of this study show that MutS tetramers increase incision efficiency compared to MutS dimers. On circular DNA, crosslinked MutS tetramers showed two-fold higher incision efficiency than wild-type MutS whereas activity of dimeric MutS D835R was two-fold lower (Fig. 3). In the absence of ATP, the crosslinked MutS tetramer has a stronger affinity to mismatch DNA than both wild-type and dimeric MutS, as shown by its apparent dissociation constant (K_D^{app}) of 6.4 nM (34) compared to wild-type MutS (K_D^{app} of 49 nM) or MutS D835R (K_D^{app} 37 nM) (34), which may explain the increased rate of incision by the tetramer. However, for MutS wild type and the D835R dimer, incision rates do not correlate with affinities for DNA. The difference in incision efficiency observed between oligomeric states on circular DNA is likely not solely due to differences in binding affinity but may be further modulated by the presence of ATP as well as differential kinetics of association and dissociation, as suggested previously (34).

Our results on linear DNA show that, unlike for wild-type MutS, increasing the concentration of the obligate dimer from 10 nM to 200 nM did not greatly improve the incision efficiency (Fig. 3). The lack of activity on linear DNA indicates that MutS dimers rapidly slide off the DNA ends while diffusing along the DNA helix. Efficient incision with MutS D835R was only observed when both MutS and MutL were simultaneously increased to at least 100 nM. In this condition, the high concentration of MutS will allow for the rapid binding of MutS to the DNA and result in multiple MutS and MutL sliding clamps moving along the 3 kb DNA molecule (55). MutL has been shown to restrict (10) or slow (44) the diffusion of MutS along the DNA. The predicted mean diffusion constant for the MutS dimer (5.2 ± 0.02) × 10^{-3} $\mu m^2/s$), fitted from experiments performed at high MutL concentration (Fig. 4), is relatively low (scanning approximately 300 bp in one second) compared to the length of the substrate. This diffusion constant is approximately 10 times lower than the experimentally determined value for the MutS dimer ((4.3 ± 1.6) × 10^{-2} $\mu m^2/s$) (44) but agrees well with the experimental values for the MutS dimer in complex with MutL ((4 ± 2) × 10^{-3} $\mu m^2/s$) and MutL and MutH ((5 ± 3) × 10^{-3} $\mu m^2/s$) (44). This suggests that under our experimental conditions, either MutS-MutL or MutS-MutL-MutH complexes are the predominant diffusive species on the DNA.

We note that our effective diffusion constant could also be a combination of the diffusion constants of the oscillating MutS-MutL-MutH complex and dissociated MutS clamp and MutL-MutH clamp species (56); however, our analytical model captures the incision data without including this oscillating behavior. Nevertheless, we have previously reported that, according to our experiments using roadblocks placed in between mismatch and GATC sites, the MutL-MutH complex is competent to initiate incision (48). Because this complex diffuses considerably faster ((4.1 ± 3.4) × 10^{-2} $\mu m^2/s$) (44) than our predicted effective diffusion constant, these observations raise the interesting possibility that the observed lag phase in incision time courses (49) is caused by the existence of long-lived, slow diffusing, inactive reaction intermediates in the pathway.

Crosslinked MutS tetramers enable activation of incision much more efficiently than MutS dimers on linear DNA. This suggests that MutS tetramers are less likely to diffuse off the DNA ends than MutS dimers, which would increase the chance of MutL binding and subsequent MutH activation. This is confirmed by our modeling, which estimates that the diffusion constant of the MutS tetramer ((1.4 ± 0.06) ×

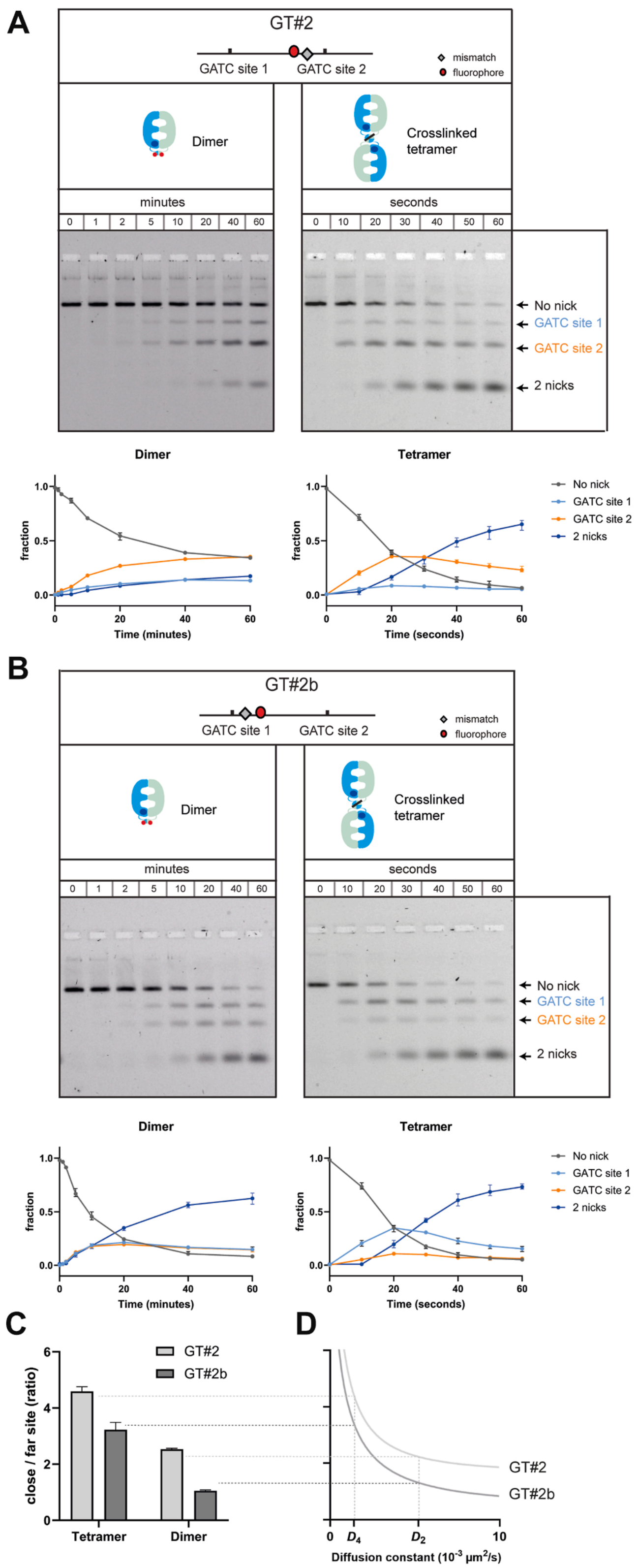

Figure 4. MutS tetramers increase preference for GATC site closest to the mismatch. Time courses (in minutes for MutS dimer, in seconds for MutS tetramer) for strand incision by 10 nM MutS, 500 nM MutL and 250 nM MutH on 0.5 nM 3 kb linear GT#2 and GT#2b. Reaction products were separated through gel electrophoresis under denaturing conditions and visualized using Alexa[647] fluorophore emission. Graphs show fractions containing no nick (*gray*), a nick at GATC site 1 (*light blue*), a nick at GATC site 2 (*orange*) and two nicks (*dark blue*). *A*, reactions on 0.5 nM linear GT#2 for MutS dimer (*left panel*) and MutS crosslinked tetramer (*right panel*). *B*, reactions on 0.5 nM linear GT#2b for MutS dimer (*left panel*) and MutS crosslinked tetramer (*right panel*). *C*, Bar graph showing experimentally determined site preference as indicated by ratio of incision of the close and far sites at 10 min (dimer) or at 40 s (tetramer) for GT#2 and GT#2b. *D*, curves showing simulated site preference obtained from a Fickian diffusion model as a function of the diffusion constant. Best fit values of diffusion constants of D_2 = (5.2 ± 0.02) × 10^{-3} $\mu m^2/s$ for dimeric and D_4 = (1.4 ± 0.06) × 10^{-3} $\mu m^2/s$ for tetrameric MutS on GT#2 and GT#2b are indicated on the x-axis and extrapolated into *panel C*.

10^{-3} μm^2/s) is about 4 times lower than the diffusion constant for the dimer, as well as the experimentally obtained diffusion constants of the dimeric MutS-MutL ((4 ± 2) × 10^{-3} μm^2/s) and MutS-MutL-MutH ((5 ± 3) × 10^{-3} μm^2/s) complexes (44). MutS tetramers have two DNA-binding sites, one for each dimer (34). Following clamp formation and mismatch release by one dimer, the other dimer, due to its high local concentration, can immediately bind to the vacated mismatch. After subsequent conformational switching by this second dimer, each dimer in the obligate tetramer would be able to diffuse along DNA as a sliding clamp. However, the two dimers are connected *via* a flexible linker, which restricts their individual movement within a few base pairs of each other. Due to this restriction, the diffusion constant of the tetramer would be expected to be smaller than that of a dimer. The tetramer would therefore take more time to reach the free ends of the DNA. In addition, MutS takes 3 to 4 s to switch from a mismatch-bound state to a sliding clamp configuration (21, 46). Within the cross-linked tetramer, the mismatch-bound MutS dimer that had not switch yet could serve as a tether for the diffusing MutS clamp, which would also increase the time MutS tetramers spend on DNA. This could also form a basis for MutS-mediated DNA loops with the tetramer at its base, which have previously been observed (26, 41).

Implication for the efficiency of DNA mismatch repair

We note that the *E.coli* genome is circular and that during normal DNA replication, MMR proteins will not encounter DNA ends. However, the use of free ends in our reconstituted reactions allows us to interpret the effect of these ends as a proxy for the distance that diffusing MMR proteins have travelled before incising a hemimethylated GATC site, providing us with mechanistic information about mismatch repair initiation. We showed that obligate MutS tetramers preferentially incise the GATC site close to the mismatch to a larger extent than MutS dimers and that this is due to the tetramers having a smaller diffusion constant than the dimer (Fig. 4). A small diffusion constant will keep the tetrameric MutS within the vicinity of the mismatch during the time in which the incision complex is assembled and activated. In the subsequent reaction step, in which the incised DNA daughter strand is unwound by the UvrD helicase and degraded by exonucleases, incisions that are located closer to the mismatch would lead to shorter excision tracts. Because excision is the rate-limiting step in MMR (49, 57), shorter excision tracts should lead to more efficient repair. This may be the explanation for the reported slight mutator phenotype for the obligate MutS dimer (30).

We also note that the human homologs of MutS, the MutSα and MutSβ heterodimers, have not been reported to form tetramers. Nevertheless, a recent study reported that MutSα-mismatched DNA complexes, in the presence of ATP, often contain two interacting MutSα heterodimers (29). Like the MutS tetramer, a MutSα heterotetramer would be expected to diffuse slower along the DNA backbone than the heterodimer. This would contribute to MutSα remaining close to the mismatch and activating the MutLα endonuclease in its vicinity (29), suggesting functional conservation of DNA incision close to the replication error between prokaryotic and eukaryotic species.

In conclusion, we have shown that during the initiation of *E.coli* DNA mismatch repair, tetramerization affects the functional behavior of MutS in MMR. We show that MutS tetramers increase DNA daughter strand incision efficiency. We provide functional evidence for diffusion along the DNA helix. In addition, we show that MutS tetramers have less diffusive movement on DNA than MutS dimers and provide estimated values for the diffusion constants of the activated complexes. Lastly, we propose that MutS tetramers may be important for keeping excision tracts close to the mismatch within the replicating *E.coli* genome. Further analysis of dimeric and tetrameric MutS behavior opens the door to understanding communication between mismatch recognition and daughter strand incision from the perspective of multimeric protein complexes.

Experimental procedures

Protein purification

E. coli MutS, MutL, and MutH mutants were purified and stored as described previously (7, 8, 33, 58). The crosslinked MutS tetramer was prepared and purified as previously described (34). Protein concentrations were determined spectrophotometrically ($\epsilon^{280\ nm}$ = 73,605 M^{-1} cm^{-1} for MutS, $\epsilon^{280\ nm}$ = 54,270 M^{-1} cm^{-1} for MutL, $\epsilon^{280\ nm}$ = 38,023 M^{-1} cm^{-1} for MutH).

MutH activation assay

Strand incision assays were performed with 10 nM MutS, 10 nM MutL and 5 nM MutH unless indicated otherwise and 0.5 nM Alexa^{647} labelled linear or circular hemi-methylated DNA substrate at 37 °C in standard assay buffer (25 mM HEPES KOH [pH 7.5], 150 mM KCl, 5 mM $MgCl_2$, 1 mM DTT, 10% glycerol, 100 ng/μl BSA, 0.005% Tween 20) containing 1 mM ATP. DNA substrates (GT#2, AT#2 and GT#2b) containing two hemimethylated GATC sites and a single G/T mismatch or corresponding A/T Watson-Crick base pair were generated as described previously (48, 49). Protein concentrations reflect the assumed minimal stoichiometry of one dimer MutS, one dimer MutL and one monomer MutH, except in titration experiments and allow complete substrate conversion within 5 min on circular substrate. For denaturing assays, reactions were started by adding a mixture of DNA and ATP to a mixture of MutS, MutL, and MutH. Reactions (10 μl) using linear DNA were stopped at the indicated time points by adding 40 μl stop solution containing 8 M Urea and 0.3% SDS. Reactions (10 μl) using circular DNA were heat-inactivated at 85 °C, linearized with ScaI-HF (New England Biolabs) for 15 min and mixed with 40 μl stop solution. Samples were denatured by incubation for 10 min at 85 °C and run on a 1.5% agarose gel in 1*TBE, both gel and buffer containing 40 μM chloroquine and 2 M urea. For non-denaturing assays, reactions were stopped at the indicated time points by adding

10ul stop solution containing glycerol, SDS and EDTA. Samples were run on a 1.5% agarose gel in 1*TAE with both gel and buffer containing 40 µM chloroquine.

Incision product formation separated by gel electrophoresis was monitored using a Typhoon FLA imager (Cytiva). The Alexa[647] fluorophore was excited at 633 nm and emission was passed through the Cy5 670BP30 filter. Band intensities were quantified using FIJI software (59). Fractions of substrate without nick, nicked intermediates and products containing two nicks were calculated relative to the total signal obtained from the fluorophore.

Modeling GATC site preference

To predict the probabilities of nicking the two different GATC sites as a function of diffusion constant and substrate geometry we build a probabilistic model. This model simultaneously captures the preferential GATC site incision on two linearized substrates, GT#2 and GT#2b. Our approach is similar to that of Crocker *et. al.* (56).

To predict the probability of a protein being present at a DNA position x at time t, we set up an initial-value problem for a one-dimensional diffusive process on L = 3200 bp (1.088 μm) DNA substrate. We assume a single protein is bound at mismatch position $x = \mu$ at time $t = 0$, where μ is 0.6018 μm if the substrate is GT#2 and 0.2686 μm if the substrate is GT#2B. We set the activation time for the complex to be capable of nicking (t_{act}) to be 10 sec, reflecting the previously observed lag phase in incision curves (49). We calculate the position distribution u (x, t_{act}) of this protein at activation time by solving the following Fickian diffusion initial value problem

$$\begin{cases} \dfrac{\partial u}{\partial t} = -D\,\dfrac{\partial^2 u}{\partial u^2} \\ u(0,t) = u(L,t) = 0, t \geq 0 \\ u(x,0) = \delta(x-\mu), x \in [0,L] \end{cases} \tag{1}$$

and substituting in t_{act}. Given the heat kernel

$$G(x,t) = \frac{1}{\sqrt{4\pi Dt}} \exp\left(-\frac{x^2}{4Dt}\right) \tag{2}$$

we can use the method of images to produce the absorbing boundary conditions at $x = 0$ and $x = L$ by constructing the odd infinite sum

$$u(x,t_{act}) = \sum_{N=-\infty}^{\infty} G(x-\mu+2NL,t_{act}) - G(x-\mu+2(N+1)L,t_{act}). \tag{3}$$

The above solves the initial value problem in Equation 1 and allows us to compute the probability density of finding a protein at a given position at activation time. We truncate this series at ±100 to calculate the density profile.

To compute the site preference, we compute the splitting probabilities of four events occurring to a protein starting at position x as follows; dissociating at the left free end of the DNA, hitting the left GATC site, hitting the right GATC site and dissociating at the right end. Let γ_1 = 0.2448 μm and γ_2 = 0.6120 μm denote the positions of GATC site one and two respectively. Accounting for the probability of a diffuser exiting an interval to the left or right given given its position, the splitting probabilities of hitting sites 0, γ_1, γ_2, L are dependent on the distance between x and both ends and given by

$$\begin{aligned} p_0 &= \theta(\gamma_1 - x)\frac{x-\gamma_1}{\gamma_1} \\ p_{\gamma_1} &= \theta(\gamma_1 - x)\frac{x}{\gamma_1} + \theta(x-\gamma_1)\theta(\gamma_2 - x)\frac{x-(\gamma_1-\gamma_2)}{\gamma_2-\gamma_1} \\ p_{\gamma_2} &= \theta(x-\gamma_1)\theta(\gamma_2-x)\frac{x}{\gamma_2-\gamma_1} + \theta(x-\gamma_2)\frac{x}{L-\gamma_2} \\ p_L &= \theta(x-\gamma_2)\frac{x-(L-\gamma_2)}{L-\gamma_2}. \end{aligned} \tag{4}$$

In the above, $\theta(x)$ denotes the Heaviside step function. To subsequently compute the total probability P_α of a certain site α being reached first, we integrate the splitting probability over x, resulting in

$$P_\alpha = \int_0^L p_\alpha u(x,t_{act})dx, \alpha = 0, \gamma_1, \gamma_2, L. \tag{5}$$

We then obtain the fold-change $\widehat{f}$ as a function of the diffusion constant as

$$\widehat{f}(D) = \begin{cases} \dfrac{P_{\gamma_2}}{P_{\gamma_1}} \text{ for } GT\#2 \\ \dfrac{P_{\gamma_1}}{P_{\gamma_2}} \text{ for } GT\#2B. \end{cases} \tag{6}$$

To fit the diffusion constant to the experimental site preference for the dimer on GT#2 and GT#B, we minimize the root-mean-square deviation between the experimental and simulated fold-changes as

$$D_{dimer} = \underset{D}{\operatorname{argmin}} \sqrt{\frac{1}{2} \sum_{i=GT\#2,GT\#2B} \left(\widehat{f}_i(D) - f_i^{dimer}\right)^2}, \tag{7}$$

using a Dual Annealing global minimization algorithm (60), resulting in a best-fit diffusion constant for complexes containing dimeric and tetrameric MutS. Three replicates were fit individually, and the best-fit diffusion constant range was reported.

Data availability

Software was deposited on Github at https://github.com/Romanovg185/nicking-site-preference (https://doi.org/10.5281/zenodo.15738762).

Supporting information—This article contains supporting information.

Author contributions—Y. M., R. M. G., C. L., and K. D. A. K. investigation; Y. M. and C. L. validation; Y. M. and R. M. G visualization; Y. M. and R. M. G. writing–original draft; R. M. G., M. D., and J. H. G. L. methodology; K. D. A. K. and P. F. resources; P. F., R. K., M. D., and J. H. G. L. supervision; R. K,. M. D., and J. H. G. L. writing–review and editing; R. K. and J. H. G. L. funding acquisition; J. H. G. L. conceptualization.

Funding and additional information—This study was supported by the Netherlands Organisation for Scientific Research (NWO) (ECHO.016.001), by the Oncode Institute, which is partly financed by the Dutch Cancer Society (KWF), and by Josephine Nefkens Cancer Program infrastructure support.

Conflict of interest—The authors declare that they do not have any conflicts of interest with the content of this article.

Abbreviations—The abbreviations used are: MMR, mismatch repair; ss, single-stranded.

References

1. Kunkel, T. A., and Erie, D. A. (2005) DNA mismatch repair. *Annu. Rev. Biochem.* **74**, 681–710
2. Jiricny, J. (2013) Postreplicative mismatch repair. *Csh Perspect. Biol.* **5**, a012633
3. Heinen, C. D. (2016) Mismatch repair defects and Lynch syndrome: the role of the basic scientist in the battle against cancer. *DNA Repair (Amst)* **38**, 127–134
4. Lahue, R. S., Au, K. G., and Modrich, P. (1989) DNA mismatch correction in a defined system. *Science* **245**, 160–164
5. Su, S. S., and Modrich, P. (1986) Escherichia coli mutS-encoded protein binds to mismatched DNA base pairs. *Proc. Natl. Acad. Sci. U. S. A.* **83**, 5057–5061
6. Lamers, M. H., Perrakis, A., Enzlin, J. H., Winterwerp, H. H., de Wind, N., and Sixma, T. K. (2000) The crystal structure of DNA mismatch repair protein MutS binding to a G x T mismatch. *Nature* **407**, 711–717
7. Groothuizen, F. S., Winkler, I., Cristovao, M., Fish, A., Winterwerp, H. H., Reumer, A., *et al*. (2015) MutS/MutL crystal structure reveals that the MutS sliding clamp loads MutL onto DNA. *Elife* **4**, e06744
8. Lebbink, J. H., Fish, A., Reumer, A., Natrajan, G., Winterwerp, H. H., and Sixma, T. K. (2010) Magnesium coordination controls the molecular switch function of DNA mismatch repair protein MutS. *J. Biol. Chem.* **285**, 13131–13141
9. Qiu, R., DeRocco, V. C., Harris, C., Sharma, A., Hingorani, M. M., Erie, D. A., *et al*. (2012) Large conformational changes in MutS during DNA scanning, mismatch recognition and repair signalling. *EMBO J.* **31**, 2528–2540
10. Qiu, R., Sakato, M., Sacho, E. J., Wilkins, H., Zhang, X., Modrich, P., *et al*. (2015) MutL traps MutS at a DNA mismatch. *Proc. Natl. Acad. Sci. U. S. A.* **112**, 10914–10919
11. Grilley, M., Welsh, K. M., Su, S. S., and Modrich, P. (1989) Isolation and characterization of the Escherichia coli mutL gene product. *J. Biol. Chem.* **264**, 1000–1004
12. Galio, L., Bouquet, C., and Brooks, P. (1999) ATP hydrolysis-dependent formation of a dynamic ternary nucleoprotein complex with MutS and MutL. *Nucleic Acids Res.* **27**, 2325–2331
13. Acharya, S., Foster, P. L., Brooks, P., and Fishel, R. (2003) The coordinated functions of the E. coli MutS and MutL proteins in mismatch repair. *Mol. Cell* **12**, 233–246
14. Au, K. G., Welsh, K., and Modrich, P. (1992) Initiation of methyl-directed mismatch repair. *J. Biol. Chem.* **267**, 12142–12148
15. Hall, M. C., and Matson, S. W. (1999) The Escherichia coli MutL protein physically interacts with MutH and stimulates the MutH-associated endonuclease activity. *J. Biol. Chem.* **274**, 1306–1312
16. Langle-Rouault, F., Maenhaut-Michel, G., and Radman, M. (1987) GATC sequences, DNA nicks and the MutH function in Escherichia coli mismatch repair. *EMBO J.* **6**, 1121–1127
17. Barras, F., and Marinus, M. G. (1989) The great GATC: DNA methylation in E. coli. *Trends Genet.* **5**, 139–143
18. Campbell, J. L., and Kleckner, N. (1990) E. coli oriC and the dnaA gene promoter are sequestered from dam methyltransferase following the passage of the chromosomal replication fork. *Cell* **62**, 967–979
19. Welsh, K. M., Lu, A. L., Clark, S., and Modrich, P. (1987) Isolation and characterization of the Escherichia coli mutH gene product. *J. Biol. Chem.* **262**, 15624–15629
20. Gradia, S., Subramanian, D., Wilson, T., Acharya, S., Makhov, A., Griffith, J., *et al*. (1999) hMSH2-hMSH6 forms a hydrolysis-independent sliding clamp on mismatched DNA. *Mol. Cell* **3**, 255–261
21. Jeong, C., Cho, W. K., Song, K. M., Cook, C., Yoon, T. Y., Ban, C., *et al*. (2011) MutS switches between two fundamentally distinct clamps during mismatch repair. *Nat. Struct. Mol. Biol.* **18**, 379–385
22. Gorman, J., Wang, F., Redding, S., Plys, A. J., Fazio, T., Wind, S., *et al*. (2012) Single-molecule imaging reveals target-search mechanisms during DNA mismatch repair. *Proc. Natl. Acad. Sci. U. S. A.* **109**, E3074–E3083
23. Bjornson, K. P., Blackwell, L. J., Sage, H., Baitinger, C., Allen, D., and Modrich, P. (2003) Assembly and molecular activities of the MutS tetramer. *J. Biol. Chem.* **278**, 34667–34673
24. Manelyte, L., Urbanke, C., Giron-Monzon, L., and Friedhoff, P. (2006) Structural and functional analysis of the MutS C-terminal tetramerization domain. *Nucleic Acids Res.* **34**, 5270–5279
25. Lamers, M. H., Georgijevic, D., Lebbink, J. H., Winterwerp, H. H., Agianian, B., de Wind, N., *et al*. (2004) ATP increases the affinity between MutS ATPase domains. Implications for ATP hydrolysis and conformational changes. *J. Biol. Chem.* **279**, 43879–43885
26. Jiang, Y., and Marszalek, P. E. (2011) Atomic force microscopy captures MutS tetramers initiating DNA mismatch repair. *EMBO J.* **30**, 2881–2893
27. Monti, M. C., Cohen, S. X., Fish, A., Winterwerp, H. H., Barendregt, A., Friedhoff, P., *et al*. (2011) Native mass spectrometry provides direct evidence for DNA mismatch-induced regulation of asymmetric nucleotide binding in mismatch repair protein MutS. *Nucleic Acids Res.* **39**, 8052–8064
28. Gupta, S., Gellert, M., and Yang, W. (2011) Mechanism of mismatch recognition revealed by human MutSbeta bound to unpaired DNA loops. *Nat. Struct. Mol. Biol.* **19**, 72–78
29. Bradford, K. C., Wilkins, H., Hao, P., Li, Z. M., Wang, B., Burke, D., *et al*. (2020) Dynamic human MutSalpha-MutLalpha complexes compact mismatched DNA. *Proc. Natl. Acad. Sci. U. S. A.* **117**, 16302–16312
30. Calmann, M. A., Nowosielska, A., and Marinus, M. G. (2005) Separation of mutation avoidance and antirecombination functions in an Escherichia coli mutS mutant. *Nucleic Acids Res.* **33**, 1193–1200
31. Calmann, M. A., Nowosielska, A., and Marinus, M. G. (2005) The MutS C terminus is essential for mismatch repair activity in vivo. *J. Bacteriol.* **187**, 6577–6579
32. Mendillo, M. L., Putnam, C. D., and Kolodner, R. D. (2007) Escherichia coli MutS tetramerization domain structure reveals that stable dimers but not tetramers are essential for DNA mismatch repair in vivo. *J. Biol. Chem.* **282**, 16345–16354
33. Tham, K. C., Hermans, N., Winterwerp, H. H., Cox, M. M., Wyman, C., Kanaar, R., *et al*. (2013) Mismatch repair inhibits homeologous recombination via coordinated directional unwinding of trapped DNA structures. *Mol. Cell* **51**, 326–337
34. Groothuizen, F. S., Fish, A., Petoukhov, M. V., Reumer, A., Manelyte, L., Winterwerp, H. H., *et al*. (2013) Using stable MutS dimers and tetramers

to quantitatively analyze DNA mismatch recognition and sliding clamp formation. *Nucleic Acids Res.* **41**, 8166–8181
35. Hall, M. C., and Kunkel, T. A. (2001) Purification of eukaryotic MutL homologs from Saccharomyces cerevisiae using self-affinity technology. *Protein Expr. Purif.* **21**, 333–342
36. Hall, M. C., Shcherbakova, P. V., Fortune, J. M., Borchers, C. H., Dial, J. M., Tomer, K. B., *et al.* (2003) DNA binding by yeast Mlh1 and Pms1: implications for DNA mismatch repair. *Nucleic Acids Res.* **31**, 2025–2034
37. Elez, M., Radman, M., and Matic, I. (2012) Stoichiometry of MutS and MutL at unrepaired mismatches in vivo suggests a mechanism of repair. *Nucleic Acids Res.* **40**, 3929–3938
38. Hombauer, H., Campbell, C. S., Smith, C. E., Desai, A., and Kolodner, R. D. (2011) Visualization of eukaryotic DNA mismatch repair reveals distinct recognition and repair intermediates. *Cell* **147**, 1040–1053
39. Junop, M. S., Obmolova, G., Rausch, K., Hsieh, P., and Yang, W. (2001) Composite active site of an ABC ATPase: MutS uses ATP to verify mismatch recognition and authorize DNA repair. *Mol. Cell* **7**, 1–12
40. Schofield, M. J., Nayak, S., Scott, T. H., Du, C., and Hsieh, P. (2001) Interaction of Escherichia coli MutS and MutL at a DNA mismatch. *J. Biol. Chem.* **276**, 28291–28299
41. Allen, D. J., Makhov, A., Grilley, M., Taylor, J., Thresher, R., Modrich, P., *et al.* (1997) MutS mediates heteroduplex loop formation by a translocation mechanism. *EMBO J.* **16**, 4467–4476
42. Blackwell, L. J., Martik, D., Bjornson, K. P., Bjornson, E. S., and Modrich, P. (1998) Nucleotide-promoted release of hMutSalpha from heteroduplex DNA is consistent with an ATP-dependent translocation mechanism. *J. Biol. Chem.* **273**, 32055–32062
43. Gradia, S., Acharya, S., and Fishel, R. (1997) The human mismatch recognition complex hMSH2-hMSH6 functions as a novel molecular switch. *Cell* **91**, 995–1005
44. Liu, J., Hanne, J., Britton, B. M., Bennett, J., Kim, D., Lee, J. B., *et al.* (2016) Cascading MutS and MutL sliding clamps control DNA diffusion to activate mismatch repair. *Nature* **539**, 583–587
45. Gorman, J., Plys, A. J., Visnapuu, M. L., Alani, E., and Greene, E. C. (2010) Visualizing one-dimensional diffusion of eukaryotic DNA repair factors along a chromatin lattice. *Nat. Struct. Mol. Biol.* **17**, 932–938
46. Cho, W. K., Jeong, C., Kim, D., Chang, M., Song, K. M., Hanne, J., *et al.* (2012) ATP alters the diffusion mechanics of MutS on mismatched DNA. *Structure* **20**, 1264–1274
47. Pluciennik, A., and Modrich, P. (2007) Protein roadblocks and helix discontinuities are barriers to the initiation of mismatch repair. *Proc. Natl. Acad. Sci. U. S. A.* **104**, 12709–12713
48. Mardenborough, Y. S. N., Nitsenko, K., Laffeber, C., Duboc, C., Sahin, E., Quessada-Vial, A., *et al.* (2019) The unstructured linker arms of MutL enable GATC site incision beyond roadblocks during initiation of DNA mismatch repair. *Nucleic Acids Res.* **47**, 11667–11680
49. Hermans, N., Laffeber, C., Cristovao, M., Artola-Boran, M., Mardenborough, Y., Ikpa, P., *et al.* (2016) Dual daughter strand incision is processive and increases the efficiency of DNA mismatch repair. *Nucleic Acids Res.* **44**, 6770–6786
50. London, J., Martin-Lopez, J., Yang, I., Liu, J., Lee, J. B., and Fishel, R. (2021) Linker domain function predicts pathogenic MLH1 missense variants. *Proc. Natl. Acad. Sci. U. S. A.* **118**, e2019215118
51. Baitinger, C., Burdett, V., and Modrich, P. (2003) Hydrolytically deficient MutS E694A is defective in the MutL-dependent activation of MutH and in the mismatch-dependent assembly of the MutS.MutL.heteroduplex complex. *J. Biol. Chem.* **278**, 49505–49511
52. Selmane, T., Schofield, M. J., Nayak, S., Du, C., and Hsieh, P. (2003) Formation of a DNA mismatch repair complex mediated by ATP. *J. Mol. Biol.* **334**, 949–965
53. Biswas, I., Ban, C., Fleming, K. G., Qin, J., Lary, J. W., Yphantis, D. A., *et al.* (1999) Oligomerization of a MutS mismatch repair protein from Thermus aquaticus. *J. Biol. Chem.* **274**, 23673–23678
54. Bjornson, K. P., Allen, D. J., and Modrich, P. (2000) Modulation of MutS ATP hydrolysis by DNA cofactors. *Biochemistry* **39**, 3176–3183
55. Hanne, J., Britton, B. M., Park, J., Liu, J., Martin-Lopez, J., Jones, N., *et al.* (2018) MutS homolog sliding clamps shield the DNA from binding proteins. *J. Biol. Chem.* **293**, 14285–14294
56. Crocker, K., London, J., Medina, A., Fishel, R., and Bundschuh, R. (2021) Evolutionary advantage of a dissociative search mechanism in DNA mismatch repair. *Phys. Rev. E* **103**, 052404
57. Hasan, A. M., and Leach, D. R. (2015) Chromosomal directionality of DNA mismatch repair in Escherichia coli. *Proc. Natl. Acad. Sci. U. S. A.* **112**, 9388–9393
58. Natrajan, G., Lamers, M. H., Enzlin, J. H., Winterwerp, H. H., Perrakis, A., and Sixma, T. K. (2003) Structures of Escherichia coli DNA mismatch repair enzyme MutS in complex with different mismatches: a common recognition mode for diverse substrates. *Nucleic Acids Res.* **31**, 4814–4821
59. Schindelin, J., Arganda-Carreras, I., Frise, E., Kaynig, V., Longair, M., Pietzsch, T., *et al.* (2012) Fiji: an open-source platform for biological-image analysis. *Nat. Methods* **9**, 676–682
60. Virtanen, P., Gommers, R., Oliphant, T. E., Haberland, M., Reddy, T., Cournapeau, D., *et al.* (2020) SciPy 1.0: fundamental algorithms for scientific computing in Python. *Nat. Methods* **17**, 261–272